Testing Charge-, Sign- and Energy-Dependence of Cosmic-Ray Solar Modulation with AMS-02 observations during cycle 24

Submitted by
Ian McKinnon

Physics

To
The Honors College
Oakland University

In partial fulfillment of the
Requirements to graduate from
The Honors College

Mentor: Dr. Ilias Cholis
Physics Department
Oakland University

April 1, 2022

1 Abstract

Our basic theoretical understanding of the sources of cosmic rays and their propagation through the interstellar medium is hindered by the Sun, that through the solar wind affects the observed cosmic-ray spectra.This effect is known as solar modulation. However recently released cosmic-ray data and publicly available measurements of the solar wind properties from ACS and the Wilcox observatory allow us to test the analytical modeling of the time-, charge- and energy-dependence of solar modulation. Using the well established time-dependence of solar modulation we establish evidence for its charge and energy dependence.

2 Introduction

The Sun produces a time-varying stream of charged particles known as the solar wind that extends far beyond Pluto and encompasses our solar system. This bubble-like region is called the Heliosphere. The solar wind and its embedded magnetic field known as Heliospheric Magnetic Field (HMF) can have a strong effect on cosmic rays (CR) entering from the interstellar medium (ISM), the space outside the Heliosphere and between stellar systems in our Galaxy. CRs propagating through the Heliosphere can get deflected and lose energy by interacting with the HMF. This effect, known as solar modulation of cosmic rays, causes the CRs observed at Earth to have significant variations in their intensity and energy. With current CR observations the statistical errors associated with the detected fluxes are now much smaller than the systematic uncertainties associated with CR propagation, including solar modulation. Given this high precision era for CRs, it is important to properly understand how the Sun influences their spectra in order to make reliable inferences on how CRs are produced and propagate throughout the Milky Way.

To include the time-evolution of the HMF and its impact on solar modulation we use ongoing observations from the Advanced Composition Explorer(*ACE*) [1, 2]. Magnetometer and the solar Wind electron Proton Alpha Monitor (SWEPAM)

[3]. We also use information on the value of the tilt angle of the heliospheric current sheet (HCS) -associated to the time-varying morphology of the HMF- from publicly available model-parameters from the Wilcox Solar Observatory [4]. The tilt angle of the heliospheric current sheet (HCS) and the magnitude of the HMF at the position of Earth have strong correlation to the cosmic-ray solar modulation and are well observed using *ACE* data and the Wilcox Observatory (See Figure 1).

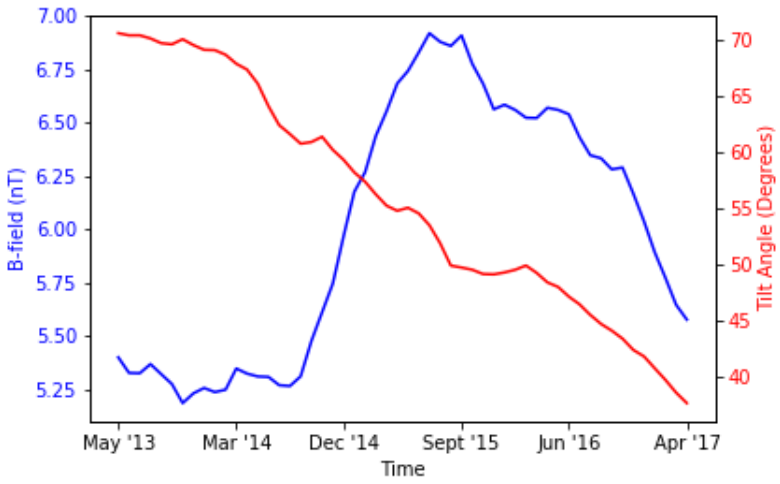

Figure 1: Magnitude of the solar magnetic field (blue line and axis) and tilt angle (red line and axis) of the heliospheric magnetic field over time. Data from [2] and [4].

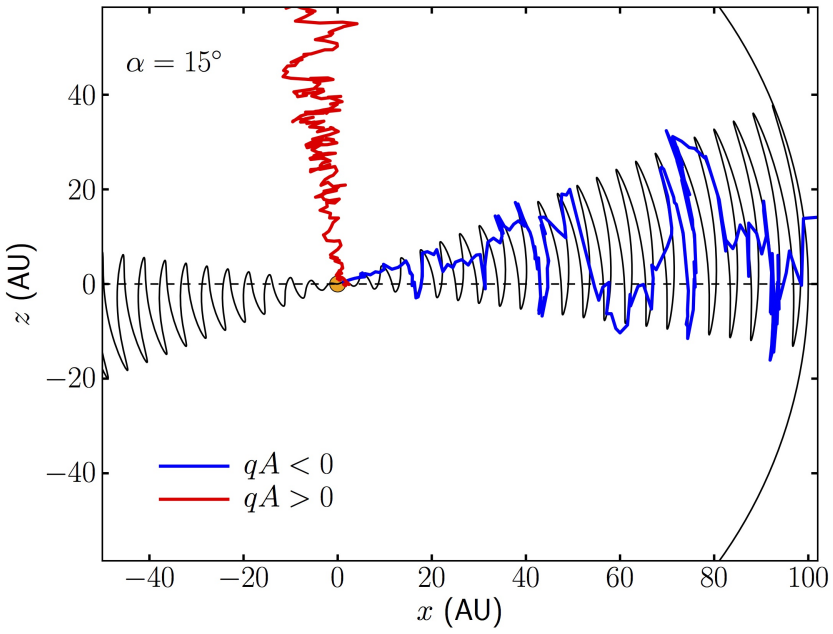

Figure 2: Modeling the charge dependence of solar modulation on cosmic rays. The red line represents propagation through the solar poles. The blue line represents propagation through the HCS. Figure from [5].

As particles enter the Heliosphere they are deflected through the magnetic field and depending on their charge propagate through different regions of the HMF. thus there is also a dependency on the charge q of a cosmic ray, relative to the current solar magnetic polarity A. As shown in Figure 2, when $qA < 0$, particles propagate mostly through the HCS, while when $qA > 0$, particles propagate mostly through the solar magnetic poles. In our work we model the effect of the different paths that CRs of opposite charge follow as they propagate to the Earth.

3 The Physics

The Sun is made up almost entirely of Hydrogen and Helium and the fusion of Hydrogen in the Sun's core is how the Sun produces its energy. This energy radiates outward from the core, travelling to the surface of the Sun, called the photosphere, and gets accelerated as it travels through the corona, the Sun's upper atmosphere. It leaves the Sun as a stream of charged particles known as the solar wind. The solar wind has a composition similar to the solar plasma found in the photosphere: mostly ionized Hydrogen i.e. electrons and protons, about 8 percent Helium, and trace amounts of heavy ions. It is important to note that the solar wind is a jet of plasma, unrelated to Earth wind. The space that these winds propagate through is called the interplanetary medium. As these winds propagate outward from the Sun, the velocities of the particles gradually slow down until they can no longer propagate outwards. This forms an elliptical bubble known as the Heliosphere that encompasses the Solar System and extends out far beyond the planets, illustrated in Fig 3 below. Similar to the interplanetary medium, the space between stellar systems is known as the interstellar medium or the ISM. Interstellar wind made up of particles from a variety of sources propagate through the ISM with a wide energy spectra. However, the interstellar wind is much less dense than the solar wind and tends to be much more energetic. The Heliosphere

ends where the solar wind can no longer propagate outwards due to the pressure of the interstellar wind pushing back against its propagation. This region is known as the Heliopause.

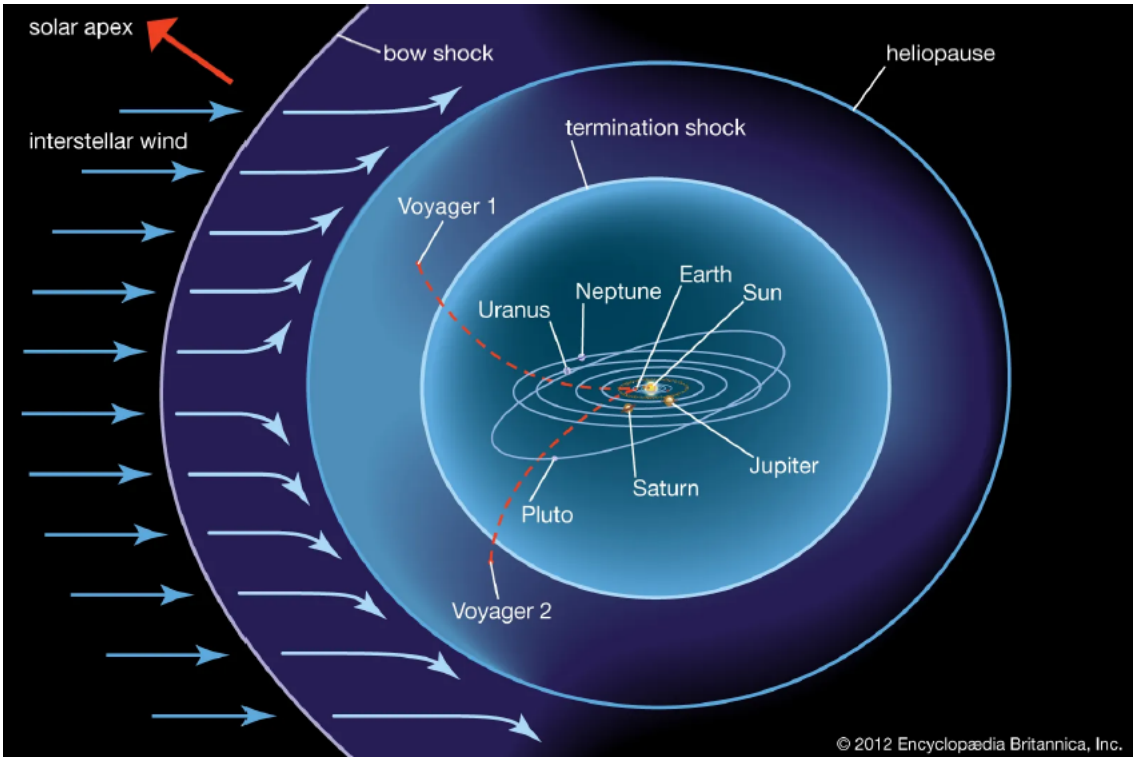

Figure 3: Illustration of the heliosphere from [6].

Since the solar wind is composed of charged particles, the movement of these particles creates a strong magnetic field that propagates out the Sun, primarily at its poles. This is known as the Heliospheric Current Sheet (HCS) which plays a very important role in solar modulation. Roughly every 11 years, the Sun's magnetic poles will gradually reverse. The flipping of the Sun's polarity twice marks a solar cycle, which is the time frame of this paper. The Sun also rotates about an axis, similar to the Earth. Each rotation is exactly 27 days and is known as a Bartel Rotation. Each rotation is given a number corresponding to the number of rotations since February 8, 1832. Similar to the Earth, the axis of the solar magnetic poles are on an angle with the Sun's axis of rotation. This is denoted as the solar tilt angle. Because the solar wind propagates radially outwards from the poles, as the Sun rotates, the HCS forms a spiral shape as it gets farther away from the Sun, as seen in Figure 4.

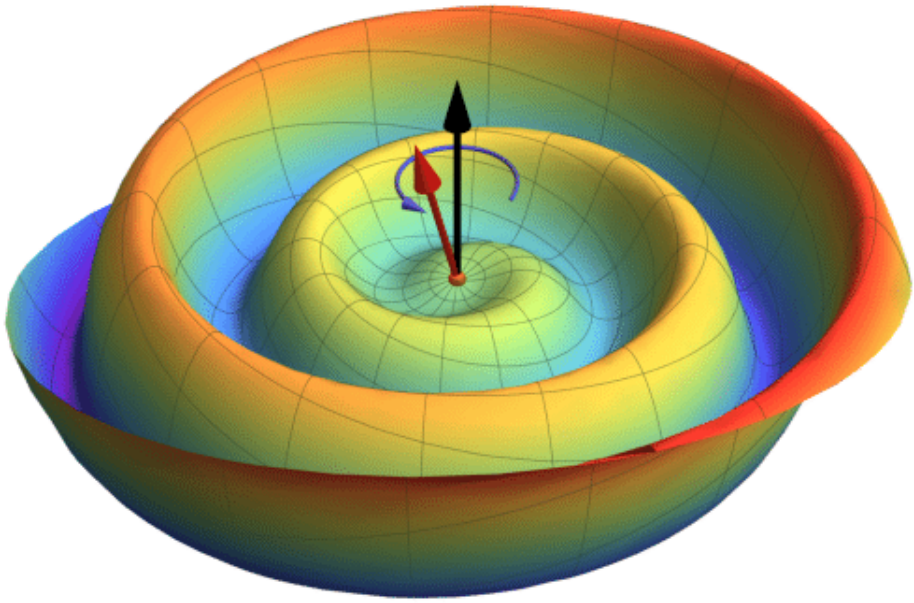

Figure 4: Graphical representation of the Heliospheric Current Sheet. The axis of rotation represented as a black vector, the direction of rotation represented as a blue vector, and the solar magnetic field axis represented as a red vector. Figure from [7]

Over time, as particles propagate inward from the ISM, the energy of a particle is gradually reduced as it travels against the solar wind. Since the solar wind differs depending on where it is in the Heliosphere, otherwise known as anisotropic, the path that a particle takes inside the Heliosphere will effect how much energy is lost. This energy loss due to solar effects is known as solar modulation. The energy spectra of particles in the ISM gets modulated by the Sun, so when the energy of particles are measured at Earth, the energy spectra is measurably different, and is reduced unequally across the spectra. Knowing exactly

what and how these particles are reduced as they travel through the Heliosphere will give us a better understanding of the Sun and its effects on particles entering the solar system.

4 Methodology

The analytic treatment of solar modulation employs the "force-field" approximation [8]. The effect of solar modulation is that the kinetic energy E_{kin} of each particle is reduced by $|Z|e\Phi$, where Φ is the modulation potential, generally on the order of 0.1 - 1.0 GV, and $|Z|e$ is the absolute charge of the CR. The resulting effect of the modulation potential on the CR spectrum can be written as:

$$\frac{dN^{\oplus}}{dE_{kin}}(E_{kin}) = \frac{(E_{kin}+m)^2 - m^2}{(E_{kin}+m+|Z|e\Phi)^2 - m^2} \frac{dN^{ISM}}{dE_{kin}}(E_{kin}+|Z|e\Phi) \tag{1}$$

where E_{kin} is the observed kinetic energy and the subscripts "*ISM*" and "$\oplus$" denote values in the interstellar medium and at the location of Earth, respectively. Typically, the value of Φ is fitted to the CR observations without a prediction on what its value should be at any given time nor does it account for particles of opposite charge. Moreover the value of Φ is assumed to be the same for all CRs irrespective of the energy they carry as they enter the HMF.

We start from the model of Φ used in [5]. The solar modulation potential depends on three well-studied quantities: the polarity of the solar magnetic field, the magnitude of the HMF at 1 AU, and the tilt angle of the HCS. The analytic expression for Φ is,

$$\Phi(R,t) = \phi_0 \left(\frac{|B_{tot}(t)|}{4nT} \right) + \phi_1 H(-qA(t)) \left(\frac{1+(\frac{R}{R_0})^2}{\beta(\frac{R}{R_0})^3} \right) \left(\frac{\alpha(t)}{\frac{\pi}{2}} \right)^4 . \quad (2)$$

A in the polarity of the HMF and $|B_{tot}|$ its strength as measured at Earth. α is the tilt angle of the HCS. These quantities are considered time-dependent inputs, and therefore independent of CR observables. R, β, and q are the rigidity($R \equiv \frac{p}{q}$, where p is the CR momentum), relativistic velocity, and charge of the CR, respectively. H is the Heaviside step function separating the treatment of opposite charges CRs based on the product of q and A as in Figure 2. R_0 is a reference rigidity and ϕ_0 and ϕ_1 are normalization factors. To compare to CR measurements at different times we use the *AMS-02* data from Ref. [9]. We test the fluxes of Hydrogen cosmic rays at five rigidity bins gathered from [9] and compare to the model of Eq. 2. We constrain the parameters of ϕ_0, ϕ_1 and R_0 by fitting them to the available CR data for solar cycle 24 using the era of May 2013 to May 2017.

The fluxes of Hydrogen are measured over a range of 49 Bartel's rota-

tions (apparent rotations of the Sun as viewed from Earth). Each rotation lasts about 27 days. For each of the five rigidity bins used (1.16-1.33, 1.92-2.15, 3.29-3.64, 5.37-5.90, and 9.26-10.1 GV), we divide the flux by the average flux over the entire period in order to show, in Figures 5 -9 below, the relative changes of the Hydrogen fluxes over time. At lower rigidities the time evolution of the cosmic-ray Hydrogen flux -and thus also its ratio to the averaged observed flux- is significantly more prominent. At the 1.16-1.33 GV bin the time variation is at the $-50\% + 80\%$ level, while at the 9.26-10.1 GV bin at the $\pm 5\%$ level.

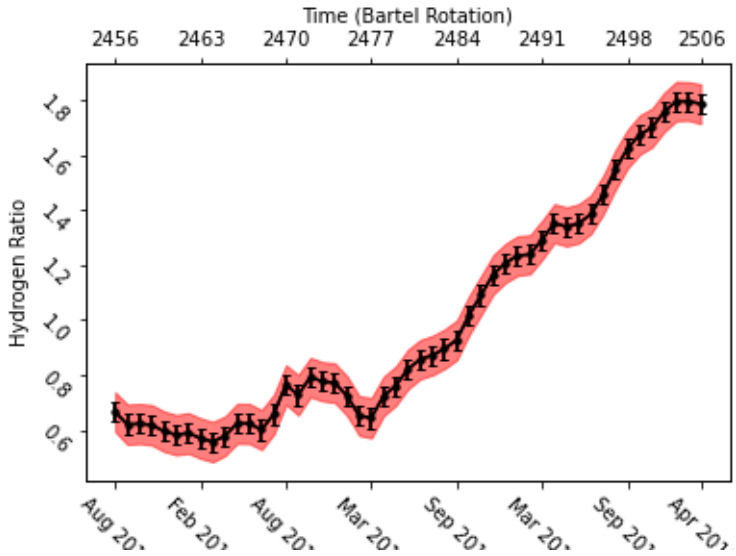

Figure 5: Time evolution of the ratio of cosmic-ray Hydrogen flux to the averaged flux within a period of 49 Bartel's cycles for the Rigidity bin of 1.16-1.33 GV

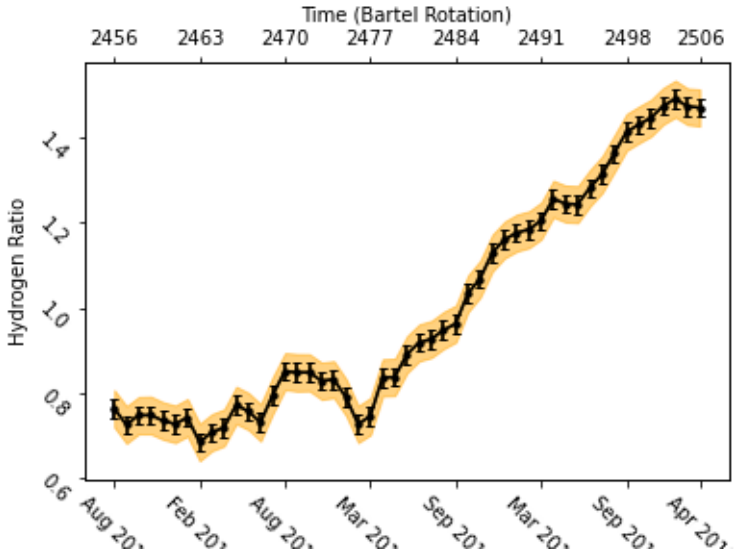

Figure 6: Time evolution of the ratio of cosmic-ray Hydrogen flux to the averaged flux within a period of 49 Bartel's cycles for the Rigidity bin of 1.92-2.15 GV

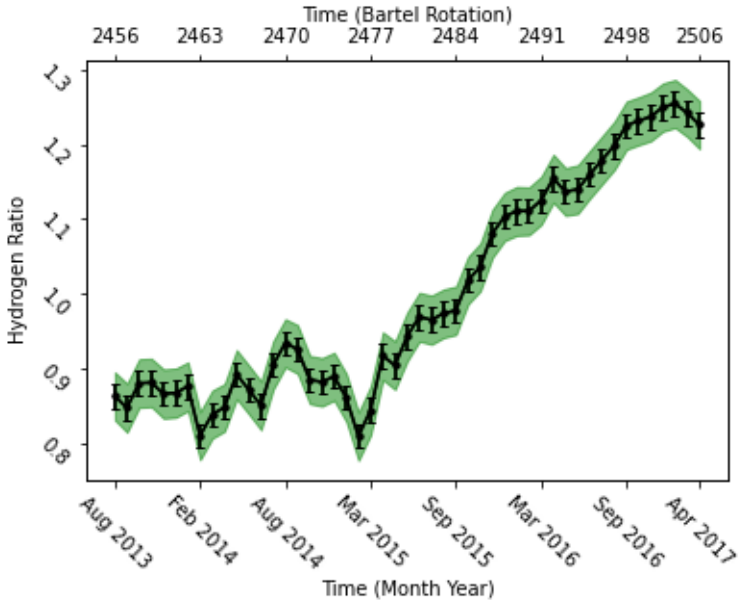

Figure 7: Time evolution of the ratio of cosmic-ray Hydrogen flux to the averaged flux within a period of 49 Bartel's cycles for the Rigidity bin of 3.29-3.64 GV

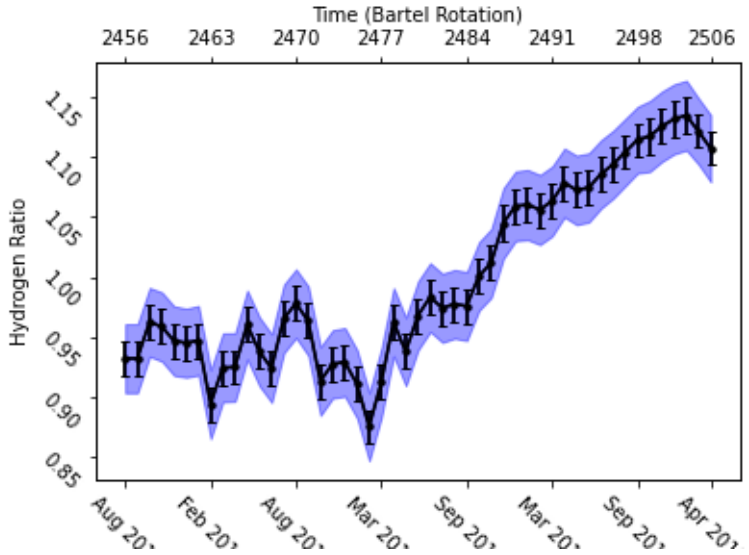

Figure 8: Time evolution of the ratio of cosmic-ray Hydrogen flux to the averaged flux within a period of 49 Bartel's cycles for the Rigidity bin of 5.37-5.90 GV

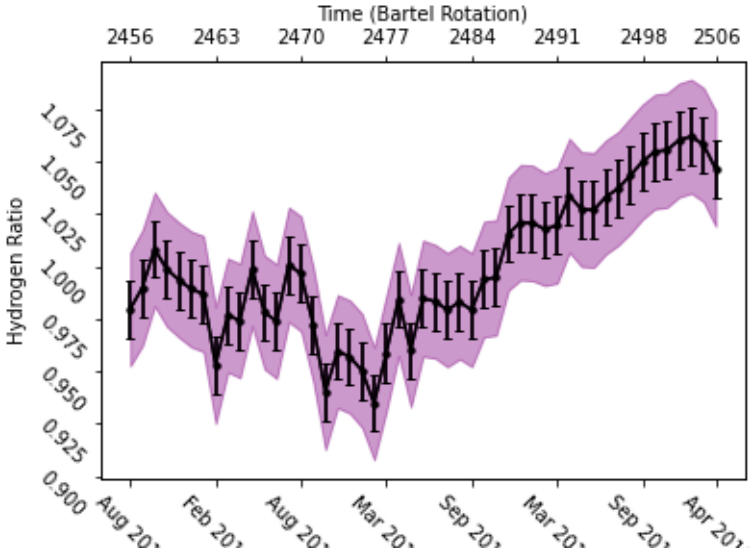

Figure 9: Time evolution of the ratio of cosmic-ray Hydrogen flux to the averaged flux within a period of 49 Bartel's cycles for the Rigidity bin of 9.26-10.1 GV

5 Results

We scan the parameter space of ϕ_0, ϕ_1, and R_0 studying the time evolution of the ratio of Hydrogen flux to its averaged value between May 2013 and May 2017. As error-bars we use the total uncertainties on the ratio, including statistical and systematic errors for [9] added in quadrature.

For the CR Hydrogen flux we calculate separately the proton and deuteron CR components by modeling the relevant ISM fluxes using the publicly available GALPROP code [11]. We break the data into two sections from BR 2456 to 2482 and from BR 2482 to 2506, as we notice a transition in the CR Hydrogen fluxes. By taking the ratio of the CR Hydrogen fluxes at different Bartel's rotations over the average of these sets of rotations we find that some of the underlying systematic modeling uncertainties of the ISM fluxes cancel out, allowing us for a more direct test of solar modulation. Moreover, the CR ISM fluxes are stable on timescales of order $\mathcal{O}(10)$ Myr at the rigidities that we test and are unaffected above rigidities of $\simeq 10$ GV.

Positively charged particles during cycle 24 mostly probe the parameter ϕ_0, while negatively charged particles also probe the values of ϕ_1 and R_0. For that reason, we also test the time evolution of the CR electron and positron fluxes as measured in [12]. However, since for the first year of the era that we test the

polarity of the HMF was still evolving, we allow for the modulation potential of positively charged particles to slowly turn off the ϕ_1-term in Eq.2. That in turn lets Hydrogen CRs constrain the values of ϕ_1 and R_0. We find that $\phi_1 > 0$ is preferred by the data, which is a clear indication for the change-dependence of solar modulation of cosmic rays [10].

The time evolution of the CR flux was incredibly difficult to model. Cosmic rays propagate through the Heliosphere in a time interval of many months to over a year. Just how long the time interval is was not certain, and a lot of time was devoted to testing various assumptions about how the fluxes evolve in time. What we found was a preference for an averaging scheme, using an average value for the solar magnetic field strength, $|B_{tot}(t)|$ and the HCS tilt angle α over the length of time it was assumed to be traveling for, instead of the value obtained from the detector which is only the average value over one Bartel rotation. The time averaging for the magnetic field strength was not assumed to equal the time averaging of the tilt angle as changes in these values are not felt instantaneously, but rather propagate through the Heliosphere at different rates. As such, we also tested for a time delay as well, where the solar values we observe when the particles are detected at Earth are significantly different from the solar values that the particles felt as they traveled, due to changes in the solar values not propagating instantly.

Based on our testing, for the first half of the time period, the averaging scheme that fit the data best was a time average of 20 Bartel rotations, or about a year and a half, for the tilt angle and 4 Bartel rotations, or about 4 months, for the magnetic field strength, with an overall time delay of 16 Bartel rotations, or about 14 months. For the second half, the averaging scheme that fit the data best was a time average of 4 Bartel rotation cycles for both the magnetic field strength and the tilt angle, with no time delay. This makes sense with our intuition, as the electrons travel mainly through the HCS during the first half, so they'll have a much longer averaging scheme and a high time delay as information travels slowly through the HCS. During the second half, they travel mainly through the poles of the Sun, travelling a much shorter distance, leading to a much smaller averaging scheme and with an insignificant time delay, as the change in magnetic field is much faster and the particle is affected by it for much shorter time periods.

Another struggle was how to accurately model the flipping of the Sun's magnetic polarity. Many different approaches to fitting the data to the model were explored. The first assumption made was that the Sun's polarity would switch linearly over several months until the the polarity had completely switched over and stabilized. This was modeled as a gradual switching off the second term in Eq.**??** from 1 to 0. Since the time it takes to switch polarity is also not certain,

various different time scales were tested. However, none of these produced good results. The next assumption was that the Sun's polarity switch could not be modeled linearly, so more complex schemes were used with the general idea being that the second term started at full strength (1) and ended at 0 when the polarity re-stabilized. However, after much time was spend and hundreds of different models were tested, even the best models created were still not good fits for the data. Since modeling the entire data set produced mediocre results, we concluded that modeling the data as one model would not work and instead modeled the first half of the data separately from the second half to better understand the effects of a transition to a new polarity. Using our best models, we constrained ϕ_0 and ϕ_1 for the first and second half of the data, as seen in Figures 10-11

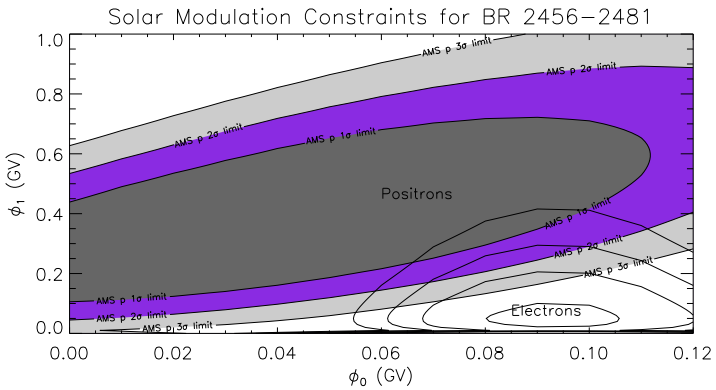

Figure 10: Constraints of the solar modulation parameters ϕ_0 and ϕ_1 for the first half of the data (BR 2456-2481) for electrons and positrons with $R_0 = 0.5$

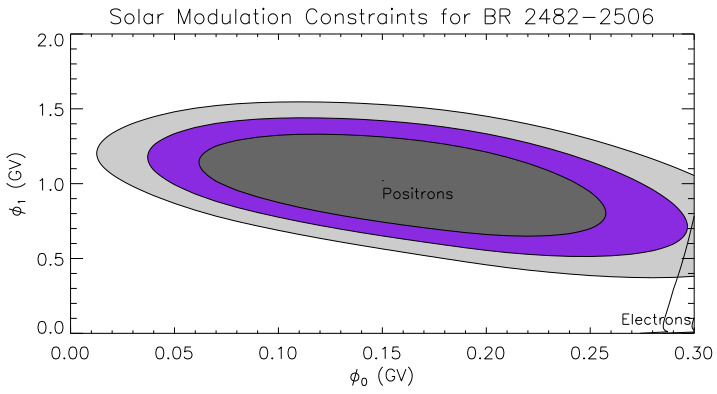

Figure 11: Constraints of the solar modulation parameters ϕ_0 and ϕ_1 for the second half of the data (BR 2482-2506) for electrons and positrons with $R_0 = 0.5$

In these figures, each band represents one standard deviation farther away from the mean, and are constrained at $R_0 = 0.5$. For each half of the data, the constraints on ϕ_0 and ϕ_1 are shown for positrons and electrons separately. For the first half of the data, positrons and electrons agree on their constraints at the 2σ level. However, for the second half of the data, they do not agree, with the electron constraints centered at values not shown in the figure. The constraints of these particles should agree, so a large disagreement between the two particles could indicate physics not accounted for in our model or an effect that is different than expected. However, the disagreement between positrons and electrons is not large enough to conclude that new physics is at play.

This research can be extended by analyzing the energy spectra of other cosmic ray particles to further constrain the ϕ_0 and ϕ_1 parameters. The reference rigidity was taken to be 0.5 as this was the value that produced the most consistent results with the data. Placing stricter constraints on the reference rigidity can be done to extend the research as well. As data gets collected on future solar cycles, work can be done comparing ϕ_0, ϕ_1, and R_0 across various solar cycles to see if they agree or potential evolve over time.

References

[1] Smith C. W., Heureux J. L., Ness N.F., Acuña M.H., Burlaga L.F. and Scheifele J. 1998 Space Science Rev. 86, 613

[2] http://www.srl.caltech.edu/ACE/ASC/

[3] S.W.E.P.A.M. Advanced Composition Explorer http://www.swpc.noaa.gov/products/ace-real-time-solar-wind

[4] http://www.wso.standford.edu/Tilts.html

[5] Cholis I., Hooper D., Linden T. 2016 Phys. Rev. D, 93, 043016

[6] Encyclopædia Britannica, Accessed on March 28, 2022. Retrieved from https://www.britannica.com/science/heliosphere#/media/1/260084/170702

[7] Orcinha M., Tomassetti N., Barão F., Bertucci B., 2019 Journal of Physics: Conference Series. 1181. 012013. 10.1088/1742-6596/1181/1/012013.

[8] Gleeson L. J. and Axford W. I. 1968 Astrophysical Journal, 154, 1011

[9] Aguilar et al., AMS Collaboration 2018 Phys. rev Lett. 121, 051101

[10] Cholis I., McKinnon I. in preparation

[11] Strong A., Moskalenko I.V. 1998 Astrophysical Journal, 509, 212

[12] Aguilar et al., AMS Collaboration 2018 Phys. rev Lett. 121, 051102